Masses and Charge Radii of $^{17-22}$Ne and the Two-Proton-Halo Candidate ^{17}Ne

W. Geithner,[1] T. Neff,[2] G. Audi,[3] K. Blaum,[1,2,*] P. Delahaye,[4] H. Feldmeier,[2] S. George,[1,2] C. Guénaut,[3] F. Herfurth,[2]
A. Herlert,[4,5] S. Kappertz,[1] M. Keim,[1] A. Kellerbauer,[4,*] H.-J. Kluge,[2,6] M. Kowalska,[4] P. Lievens,[7] D. Lunney,[3]
K. Marinova,[8] R. Neugart,[1] L. Schweikhard,[5] S. Wilbert,[1] and C. Yazidjian[2]

[1]*Institut für Physik, Johannes Gutenberg-Universität, 55099 Mainz, Germany*
[2]*GSI Helmholtzzentrum für Schwerionenforschung GmbH, Planckstraße 1, 64291 Darmstadt, Germany*
[3]*CSNSM-IN2P3-CNRS, 91405 Orsay-Campus, France*
[4]*Physics Department, CERN, 1211 Geneva 23, Switzerland*
[5]*Institut für Physik, Ernst-Moritz-Arndt-Universität, 17487 Greifswald, Germany*
[6]*Fakultät für Physik und Astronomie, Ruprecht-Karls-Universität, 69120 Heidelberg, Germany*
[7]*Laboratorium voor Vaste-Stoffysica en Magnetisme, Katholieke Universiteit Leuven, 3001 Leuven, Belgium*
[8]*Laboratory of Nuclear Reactions, Joint Institute of Nuclear Research, 141980 Dubna, Russia*
(Received 27 June 2008; published 19 December 2008)

High-precision mass and charge radius measurements on $^{17-22}$Ne, including the proton-halo candidate ^{17}Ne, have been performed with Penning trap mass spectrometry and collinear laser spectroscopy. The ^{17}Ne mass uncertainty is improved by factor 50, and the charge radii of $^{17-19}$Ne are determined for the first time. The fermionic molecular dynamics model explains the pronounced changes in the ground-state structure. It attributes the large charge radius of ^{17}Ne to an extended proton configuration with an s^2 component of about 40%. In ^{18}Ne the smaller radius is due to a significantly smaller s^2 component. The radii increase again for $^{19-22}$Ne due to cluster admixtures.

The structure of nuclei close to the drip lines is governed by weakly bound nucleons. While several neutron halos have been clearly identified, the criteria for establishing a proton halo are far less clear cut. The Borromean ^{17}Ne is a prominent candidate for a two-proton halo [1], which can be seen as an ^{15}O core in its ground state plus two protons in d^2 or halolike s^2 configurations.

Evidence for a halo was provided by several experiments. The first information on the ^{17}Ne wave function was an asymmetry in the first-forbidden β decay compared to the decay rate in the mirror nucleus ^{17}N [2], which was either attributed to a halo structure in the excited state of ^{17}F or to differences in the ^{17}Ne and ^{17}N wave functions due to Coulomb effects [3]. Using Glauber theory, interaction cross-section measurements [4] gave a matter radius of 2.75(7) fm, significantly larger than in ^{17}N. Two-proton emission was observed from higher-lying excited states of ^{17}Ne [5], whereas a large cross section and a narrow momentum distribution were found in two-proton removal reactions [6,7], which provided (within the Glauber model) a very large s^2 component. In contrast to the above investigations, the magnetic moment of ^{17}Ne, measured using collinear laser spectroscopy [8], was reproduced by shell-model calculations giving only a small s^2 occupation.

Shell-model descriptions of ^{17}Ne focused on the mirror asymmetric β-decay properties or the Coulomb displacement energies (CDE) compared to ^{17}N. While in [9] a dominant s^2 contribution was found, other shell-model calculations [10,11] predicted a s^2 admixture of only 20%. In three-body calculations, however, s^2 contributions

were 48% [12] and 45% [13]. Thus, there is still no consensus on a two-proton-halo formation in ^{17}Ne.

In this Letter we present precise measurements of the masses and charge radii of $^{17-22}$Ne. The charge radius of ^{17}Ne provides a test of model predictions as it depends sensitively on the halo protons. In contrast to CDEs and magnetic moments, details of core polarization are expected to be less important. It also does not rely on reaction theory, as in the case of interaction cross sections and momentum distributions. Extracting the isotope shift (IS) and the charge radius from collinear laser spectroscopy requires a precision mass measurement, which we also present, together with the masses of $^{18-22}$Ne. Finally, we compare the binding energies and charge radii to microscopic calculations performed in the fermionic molecular dynamics (FMD) approach. FMD reproduces the experimental values remarkably well and reveals large structural differences between the isotopes. We discuss the results in terms of halo and cluster structures.

The measurements were performed at ISOLDE/CERN, where Ne isotopes were produced by 1.4-GeV proton pulses impinging onto a CaO or MgO target. After diffusion out of the heated target through a cooled transfer line, suppressing less volatile elements, Ne atoms were ionized in a plasma and accelerated to 60 keV before being mass separated and delivered to the setups.

For the mass measurements Ne$^+$ ions were investigated with the ISOLTRAP setup [14]. The ions from ISOLDE were accumulated, cooled, and bunched within a linear radio frequency quadrupole ion trap filled with helium

buffer gas, and transferred to the preparation Penning trap for isobaric cleaning. The mass determination was performed in the precision Penning trap, where the cyclotron frequency $\nu_c = qB/(2\pi m)$ was measured with a time-of-flight cyclotron resonance technique. Experimental problems included isobaric contamination and losses by charge exchange with the buffer gas. Because of the short 109-ms half-life of ^{17}Ne, the measuring cycle took only 400 ms from proton impact to detection. Before and after the frequency measurement on the ion of interest, ν_c of the reference ^{22}Ne$^+$ was measured, in order to interpolate $\nu_{c,\text{ref}}$ and to obtain the frequency ratio $r = \nu_c/\nu_{c,\text{ref}}$. The experimental frequency ratios are given in Table I.

The present mass measurements continue previous ISOLTRAP experiments on $^{18-21}$Ne [16], and allow a new evaluation of the neon masses in the framework of the atomic-mass evaluation (AME) (Table I). The very accurate masses of ^{20,21}Ne and ^{16}O^{1}H served as a cross-check. The agreement with literature values gives confidence in the accuracy of the new mass values at relative uncertainties below 4×10^{-8} (including systematic uncertainties around 8×10^{-9} [14]). ^{17}Ne is the lightest nuclide investigated at ISOLTRAP so far, and its mass has been determined with a Penning trap for the first time. The mass value has been improved by a factor 50 and shifts the established 973-keV two-proton separation energy down by 40 keV. We use the precise mass of ^{17}Ne and other Ne isotopes to evaluate the isotope shifts and from these the changes in mean square charge radii.

The charge radii of $^{17-22}$Ne were investigated by collinear laser spectroscopy. Very sensitive detection, required particularly for ^{17}Ne, was based on ion counting [8]. The Ne ions delivered from ISOLDE were neutralized by near-resonant charge exchange with Na atoms, which populates mostly the metastable $3s[3/2]^{\circ}_2$ state in atomic neon. The fast atoms then interacted with laser light and in resonance were excited to the $3p[3/2]_2$ state, which either decays back to the metastable state or cascades with high probability to the $2p^6\ 1S_0$ ground state. Optical resonance was detected by discriminating between ground- and metastable-state populations, using the different cross sections for collisional ionization [17]. The ions created from

the passage of the beam through a Cl$_2$ gas target were deflected onto a tape system for β counting. Similarly, neutral atoms were counted in the forward direction for signal normalization. Stable isotopes were studied using fluorescence light detection.

Table II shows the measured isotope shifts. The systematic errors, arising from Doppler shifts, depend on the accuracy of voltage measurements and mass values. The isotope shift between isotopes with atomic numbers A, A' and masses $m_A, m_{A'}$,

$$\delta\nu_{\text{IS}}^{A,A'} = K_{\text{MS}} \frac{m_{A'} - m_A}{m_{A'}m_A} + F_{\text{el}}\delta\langle r^2\rangle^{A,A'}, \quad (1)$$

is given by the sum of the mass shift (MS) and field shift proportional to the change in the mean square charge radius $\delta\langle r^2\rangle$. K_{MS} is the mass-shift constant, and F_{el} is the electronic factor, obtained from atomic theory or empirical information. While the electronic factor can be calculated semiempirically from atomic spectroscopy data, the largely dominating mass shift has to be determined using independent information on $\delta\langle r^2\rangle$ between at least two isotopes. This is possible for neon, because rms charge radii $r_{\text{ch}} = \langle r^2\rangle^{1/2}$ are known from muonic atom x-ray spectroscopy [18] of stable $^{20-22}$Ne.

Values of $\delta\langle r^2\rangle$ are obtained from the isotope shifts by fixing the electronic factor to $F_{\text{el}} = -40(4)$ MHz/fm^2, based on the semiempirical approach (see [19]), and using Eq. (1) with the known $\delta\langle r^2\rangle^{20,21}$ and $\delta\langle r^2\rangle^{20,22}$ (King plot procedure). This has the further advantage that systematic errors on the isotope shifts, produced by voltage calibration uncertainties of the Doppler shifts, largely cancel for the radii [19]. Still, the Doppler shifts of about 30 GHz per mass unit have to be determined rather accurately because the field shifts are only at the percent level of the measured total isotope shifts of about 1 GHz. For this, the beam energy of 60 keV was calibrated to better than 0.5 eV, using the known transition frequencies of two optical resonances in Ne, induced simultaneously by beams from one laser overlapped collinearly and anticollinearly with the atom beam [20].

Direct results of the present experiment are the values of $\delta\langle r^2\rangle$ along the $^{17-22}$Ne chain given in Table II with their

TABLE I. Frequency ratios r of $^{17,19-21}$Ne from this study (relative to ^{22}Ne) and masses of $^{17-22}$Ne after a new mass evaluation, compared to literature [15] (AME'03). The new evaluation includes final data from [16], whereas the AME'03 used preliminary values of [16] prior to publication.

A	Frequency ratio r	AME'03 (μu)	New mass (μu)
17	0.773 829 869 8(261)	17 017 672(29)	17 017 714.75(57)
18		18 005 708.2(3)	18 005 708.70(39)
19	0.864 056 826 3(89)	19 001 880.2(3)	19 001 880.76(16)
20	0.909 101 007 3(89)	19 992 440.175(2)	19 992 440.1842(19)
21	0.954 638 456 4(116)	20 993 846.68(4)	20 993 846.684(41)
22	Reference	21 991 385.11(2)	21 991 385.113(18)

TABLE II. Isotope shifts and differences in mean square charge radii of $^{17-19,21-22}$Ne relative to ^{20}Ne. The $\delta\nu_{\text{IS}}$ uncertainties are statistical and [in square brackets] systematic due to acceleration voltage (uncertainty due to masses is below 0.01%). For $\delta\langle r^2\rangle$, statistical (due to IS statistical uncertainty) and systematic from MS and F_{el} analysis based on muonic atom data.

A	$\delta\nu_{\text{IS}}^{20,A}$ (MHz)	$\delta\langle r^2\rangle^{20,A}$ (fm)
17	$-3183.30(1.20)$ [3.3]	0.220(29) [123]
18	$-1995.53(62)$ [2.1]	$-0.207(15)$ [112]
19	$-947.39(74)$ [1.0]	0.017(19) [41]
21	874.94(56) [0.9]	$-0.217(14)$ [24]
22	1663.58(17) [1.7]	$-0.321(4)$ [43]

TABLE III. Matter and charge radii of Ne isotopes (in fm). FMD charge radii are calculated from the point proton radii taking the charge radii of protons and neutrons into account.

| A	r_m [21]	r_m FMD This work	r_{ch} [18]	r_{ch} This work	r_{ch} FMD This work
17	2.75(7)	2.75		3.042(21)	3.04
18	2.81(14)	2.70		2.971(20)	2.93
19	2.57(4)	2.84		3.009(9)	3.00
20	2.87(3)	2.87	3.006(5)		2.99
21	2.83(7)	2.86	2.967(4)	2.970(7)	2.96
22		2.87	2.954(4)	2.952(9)	2.94

FIG. 1 (color online).   The rms charge radii for $^{17-22}$Ne. Error bars indicate the statistical uncertainties. The systematic error limits are represented by the dotted line and the dashed line.

statistical and systematic uncertainties. The latter determine the general slope without affecting local effects between the isotopes. Absolute rms charge radii are derived using as reference $r_{ch}(^{20}\mathrm{Ne}) = 3.006(5)$ fm [18], as presented in Table III along with the known matter radii [21]. Figure 1 combines the information of Tables II and III and shows both types of uncertainties.

The pronounced structural changes reflected in the charge radii as a function of neutron number pose a challenge for theory. In a typical mean-field calculation, e.g., [22], radii vary smoothly from ^{17}Ne to ^{22}Ne and are much smaller than the experimental values. The FMD approach [23,24] allows one to include long-range correlations like halos or clusters.

FMD spans the many-body Hilbert space with nonorthogonal Slater determinants using as single-particle states Gaussian wave packets, which gives great flexibility. For ^{17,18}Ne we use a superposition of two wave packets which improves especially the description of extended s orbits. To restore the symmetries of the Hamiltonian, the intrinsic Slater determinants are projected on parity, angular momentum, and total linear momentum. Finally, in a configuration-mixing calculation we diagonalize the Hamiltonian to obtain the ground states. Individual FMD configurations are generated by minimizing the Hamiltonian expectation value for a parity projected state with respect to all the parameters of the single-particle states. For ^{17,18}Ne we find two minima that can be interpreted as essentially ^{15}O or ^{16}O cores plus two protons found mainly in s^2 or d^2 configurations. We obtain additional configurations with modified single-particle orbits by cranking down the strength of the spin-orbit force during minimization.

In ^{19}Ne the $1/2^-$ state is almost degenerate with the natural-parity $1/2^+$ ground state. The negative-parity state is related to a clustered intrinsic configuration that, due to missing reflection symmetry, can also be projected on positive parity. Therefore, calculations for $^{18-22}$Ne include also configurations optimized for negative parity. Configurations optimized for positive parity correspond mainly to shell-model configurations (^{16}O plus nucleons in the sd shell), while those optimized for negative parity represent configurations with clustering. In the shell-model
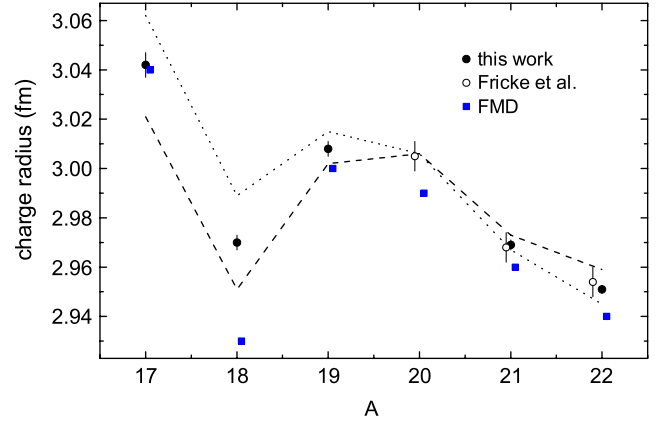
picture these correspond to excitations of the ^{16}O core. To improve the asymptotic part of the wave functions we include explicit Brink-type cluster configurations [25] with threshold energies below 10 MeV: ^{3}He-^{14}O in ^{17}Ne, ^{4}He-^{14}O in ^{18}Ne, ^{3}He-^{16}O, ^{4}He-^{15}O in ^{19}Ne, and ^{4}He$-^{16-18}$O in $^{20-22}$Ne. The wave functions for the clusters are obtained again by variation of the FMD wave functions. The effective interaction is based on the V_{UCOM} derived from the realistic Argonne V18 interaction by explicit treatment of short-range central and tensor correlations in the unitary correlation operator method [26]. It also includes a phenomenological two-body correction term fitted to reproduce binding energies and radii of doubly magic nuclei. This interaction successfully describes p- and sd-shell nuclei [27].

The FMD binding energy for ^{17}Ne is 106.66 MeV which together with the ^{15}O binding energy of 105.91 MeV leads to a two-proton separation energy of 0.75 MeV compared to the experimental value of 0.93 MeV. All other cluster
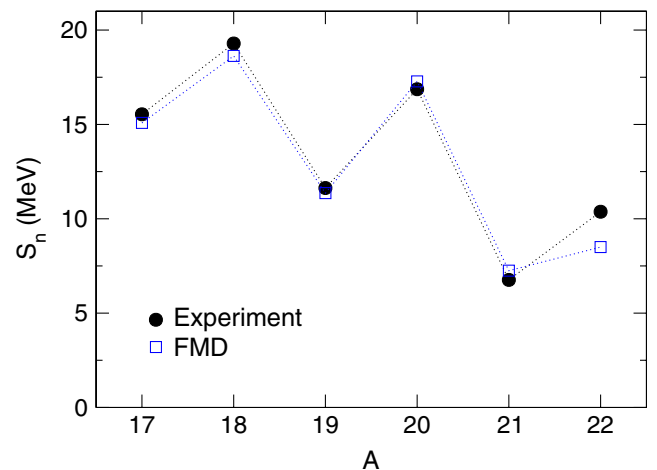

FIG. 2 (color online).   Measured and FMD one-neutron separation energies for $^{17-22}$Ne. The energy of the unbound ^{16}Ne ground state is calculated in bound-state approximation.
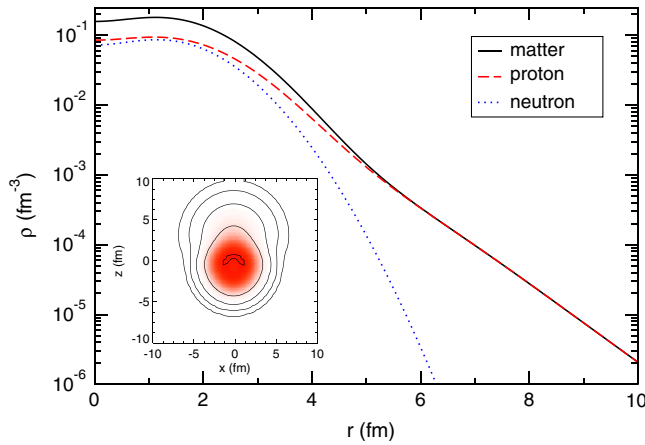
FIG. 3 (color online). Matter, proton, and neutron density distributions in the FMD ground state for ^{17}Ne. The proton skin thickness $r_p - r_n$ is 0.45 fm. The probability to find a proton at $r > 5$ fm is about 40%. Inset: Intrinsic proton density of the dominant FMD configuration, with two protons in s-d mixed orbits.

thresholds are reproduced within 0.5–1.0 MeV. The total binding energies underestimate the experimental values by about 6 MeV, reflecting the fact that the oxygen cores are essentially described only on the mean-field level. This underbinding cancels out in the one-neutron separation energies, which reproduce the experimental odd-even staggering (Fig. 2).

The FMD calculations reproduce remarkably well both the absolute values and the evolution of the measured charge radii as a function of neutron number. For ^{17}Ne FMD agrees with the measured radius, attributed to a clearly visible tail in the proton density distribution (shown together with neutron and matter distributions in Fig. 3), which implies a narrow proton momentum distribution [7] of protons relative to the compact ^{15}O core (FMD matter and charge radii: $r_m = 2.46$ fm, $r_{ch} = 2.63$ fm). Because of the missing centrifugal barrier, weakly bound s orbits are much more extended than d orbits. The charge radius of the ground state is therefore very sensitive to their relative occupation. Assuming that only the two valence protons contribute, the s^2 admixture is 42%. By slightly changing the strength of the spin-orbit force the charge radius and s^2 occupation can be tuned. The experimental error bar for $\langle r^2 \rangle$ corresponds then to s^2 occupations between 38% and 46%. An independent test of the ^{17}Ne wave function is provided by the $B(E2)$ transitions into the excited $3/2^-$ and $5/2^-$ states. We obtain $B(E2; 1/2^- \rightarrow 3/2^-) = 77e^2$ fm^4 and $B(E2; 1/2^- \rightarrow 5/2^-) = 120e^2$ fm^4, in very good agreement with the experimental values $66^{+18}_{-25}e^2$ fm^4 and $124(18)e^2$ fm^4 [28]. For ^{18}Ne with a closed $N = 8$ neutron shell, we find only about 15% s^2 admixture, explaining the much smaller charge radius. For $^{19-22}$Ne the charge radii are again larger but decrease with A. This

effect is nicely reproduced by FMD due to a different mechanism. In ^{19}Ne admixtures of spatially extended ^{16}O-^{3}He ($\ell = 0$) and ^{15}O-^{4}He ($\ell = 1$) cluster configurations in the tail of the $1/2^+$ ground-state wave function cause an increase of 0.17 fm in the charge radius compared to the FMD mean-field result. These admixtures are related to the known deformation properties and decrease with A towards ^{22}Ne for which we still find a 0.08-fm increase.

*Present address: Max-Planck-Institut für Kernphysik, Saupfercheckweg 1, 69117 Heidelberg, Germany.
[1] M. Zhukov and I. Thompson, Phys. Rev. C **52**, 3505 (1995).
[2] M. J. G. Borge *et al.*, Phys. Lett. B **317**, 25 (1993).
[3] D. J. Millener, Phys. Rev. C **55**, R1633 (1997).
[4] A. Ozawa *et al.*, Phys. Lett. B **334**, 18 (1994).
[5] T. Zerguerras *et al.*, Eur. Phys. J. A **20**, 389 (2004).
[6] R. Kanungo *et al.*, Phys. Lett. B **571**, 21 (2003).
[7] R. Kanungo *et al.*, Eur. Phys. J. A **25**, 327 (2005).
[8] W. Geithner *et al.*, Phys. Rev. C **71**, 064319 (2005).
[9] S. Nakamura *et al.*, Phys. Lett. B **416**, 1 (1998).
[10] H. T. Fortune and R. Sherr, Phys. Lett. B **503**, 70 (2001); H. T. Fortune *et al.*, Phys. Rev. C **73**, 064310 (2006).
[11] N. Michel *et al.*, Nucl. Phys. **A703**, 202 (2002).
[12] L. V. Grigorenko *et al.*, Nucl. Phys. **A713**, 372 (2003); Nucl. Phys. **A740**, 401 (2004).
[13] E. Garrido *et al.*, Nucl. Phys. **A733**, 85 (2004).
[14] M. Mukherjee *et al.*, Eur. Phys. J. A **35**, 1 (2008).
[15] G. Audi *et al.*, Nucl. Phys. **A729**, 3 (2003).
[16] K. Blaum *et al.*, Nucl. Phys. **A746**, 305 (2004).
[17] R. Neugart *et al.*, Nucl. Instrum. Methods Phys. Res., Sect. B **17**, 354 (1986).
[18] G. Fricke *et al.*, At. Data Nucl. Data Tables **60**, 177 (1995).
[19] A. Klein *et al.*, Nucl. Phys. **A607**, 1 (1996).
[20] W. Geithner *et al.*, Hyperfine Interact. **127**, 117 (2000).
[21] A. Ozawa *et al.*, Nucl. Phys. **A693**, 32 (2001).
[22] J. S. Wang *et al.*, Nucl. Phys. **A691**, 618 (2001).
[23] T. Neff and H. Feldmeier, Eur. Phys. J. Special Topics **156**, 69 (2008).
[24] R. Roth *et al.*, Nucl. Phys. **A745**, 3 (2004).
[25] D. M. Brink, in *The Alpha-Particle Model of Light Nuclei*, Proceedings of the International School of Physics "Enrico Fermi," Course XXXVI (Elsevier, Amsterdam, 1965).
[26] T. Neff and H. Feldmeier, Nucl. Phys. **A713**, 311 (2003).
[27] M. Chernykh *et al.*, Phys. Rev. Lett. **98**, 032501 (2007).
[28] M. J. Chromik *et al.*, Phys. Rev. C **66**, 024313 (2002).